Available online at www.sciencedirect.com
ScienceDirect
Journal of the European Ceramic Society 26 (2006) 3695–3704
www.elsevier.com/locate/jeurceramsoc

Oxygen transport in ferrite-based ceramic membranes: Effects of alumina sintering aid

V.V. Kharton [a,b,*], A.L. Shaula [a], F.M.M. Snijkers [c], J.F.C. Cooymans [c], J.J. Luyten [c], I.P. Marozau [a], A.P. Viskup [b], F.M.B. Marques [a], J.R. Frade [a]

[a] *Department of Ceramics and Glass Engineering, CICECO, University of Aveiro, 3810-193 Aveiro, Portugal*
[b] *Institute of Physicochemical Problems, Belarus State University, 14 Leningradskaya Str., 220050 Minsk, Belarus*
[c] *Materials Department, Flemish Institute for Technological Research (VITO), 2400 Mol, Belgium*

Received 6 July 2005; received in revised form 12 October 2005; accepted 23 October 2005
Available online 15 December 2005

Abstract

Moderate additions of Al_2O_3 to strontium ferrite-based mixed conductors, such as $SrFe_{0.7}Al_{0.3}O_{3-\delta}$ and $La_{0.2}Sr_{0.8}Fe_{0.8}Ga_{0.2}O_{3-\delta}$ with the composition close to the solid solution formation limits, make it possible to improve ceramics sinterability, to increase oxygen permeability and to decrease thermal expansion. These effects are associated with the segregation of alumina-rich phases, primarily $SrAl_2O_4$, and the formation of A-site cation-deficient perovskite. The improved properties of the $SrFe_{0.7}Al_{0.3}O_3$-based material were used to fabricate high-quality tubular membranes for methane conversion reactors. Similar enhancement in sinterability is also observed for another promising parent material of mixed-conducting membranes, $La_{0.5}Sr_{0.5}FeO_{3-\delta}$. However, extensive dissolution of Al^{3+} cations in the iron sublattice, creation of A-site vacancies and changing the La:Sr concentration ratio all lead to decreasing ionic transport in $La_{0.5}Sr_{0.5}FeO_{3-\delta}$. As a result, additions of either Al_2O_3 or $SrAl_2O_4$ have a deteriorating influence on the oxygen permeation fluxes through $La_{0.5}Sr_{0.5}FeO_3$-based ceramics.

Keywords: Perovskites; Sintering; Ionic conductivity; Membranes; $Sr(Fe, Al)O_3$; $(La, Sr)(Fe, Ga)O_3$

1. Introduction

Conversion of natural gas to synthesis gas, a mixture of CO and H_2, takes place rather effectively over the surface of a mixed oxygen-ion/electron conducting membrane, which assimilates oxidation reactions with controlled oxygen separation.[1–5] Although this technology may provide substantial economic and environmental benefits, development of membrane reactors is limited by the stringent thermomechanical and chemical demands on the membrane material, including high oxygen permeability, moderate thermal and chemically-induced expansion, mechanical and chemical stability under a wider range of oxygen chemical potentials, low cost of the raw materials and viable fabrications methods. A strong candidate to satisfy these requirements is the $SrFeO_3$-based perovskite, with Fe and Sr partially substituted by more redox- and chemically-stable cations, respectively, such as Cr, Ti, Ga and Al on the B sublattice, and La for Sr.[2,4,6–12] Particular compositions having attractive transport properties and stability are $Sr_{1-x}La_xFe_{1-y}M_yO_{3-\delta}$ (M = Ga, Cr; $x = 0.2$–0.4; $y = 0.2$–0.4), $SrFe_{0.7}Al_{0.3}O_{3-\delta}$ and $Sr_{0.5}La_{0.5}FeO_{3-\delta}$. The latter phase exhibits a maximum of electronic and oxygen ionic conductivity in the $Sr_{1-x}La_xFeO_{3-\delta}$ system; a higher strontium content without B-site doping results in oxygen vacancy ordering and deterioration of transport properties.[8] Incorporation of aluminum into the perovskite-type lattice of $SrFe_{1-y}Al_yO_{3-\delta}$ enhances the phase stability at low oxygen chemical potentials, moderately decreasing the thermal expansion and oxygen permeability within the solid solution formation range, $y = 0$–0.35.[9,10] The oxygen fluxes through ferrite ceramics showing the highest ionic transport are typically determined by both bulk ionic conductivity and surface exchange kinetics.[10,11,13] The exchange limitations play, however, a positive role under large $p(O_2)$ gradients due to kinetic stabilization of ferrite-based membrane materials thermodynamically unstable in reducing environments.[5,12–14] Namely, when the overall oxygen transport

* Corresponding author. Tel.: +351 234 370263; fax: +351 234 425300.
E-mail address: kharton@cv.ua.pt (V.V. Kharton).

0955-2219/$ – see front matter © 2005 Elsevier Ltd. All rights reserved.
doi:10.1016/j.jeurceramsoc.2005.10.013

is surface-limited, the oxygen chemical potential on the membrane permeate-side surface is always higher than that in the gas phase, thus preventing reduction.

The present work was focused on the study of sintering, microstructure and transport properties of ferrite-based perovskite ceramics with minor additions of alumina. The microstructural modification via incorporation of small amounts of highly dispersed Al_2O_3 is a well-established approach in the engineering of oxygen ion-conducting solid electrolyte materials.[15–19] While significant volume fractions of insulating aluminum oxide lead to decreasing ionic conductivity, moderate additions have no significant blocking effect, but decrease grain-boundary resistance due to "scavenging" of silica-rich impurity phases. Alumina additions to solid oxide electrolyte ceramics make it possible also to improve the mechanical strength, to suppress grain growth in the course of sintering and, often, to increase sinterability.[15–19] All these effects may be of great interest for the developments of mixed-conducting membrane materials, taking into account the stability and low costs of alumina.

2. Experimental

The powders of $SrFe_{0.7}Al_{0.3}O_{3-\delta}$ and $La_{0.5}Sr_{0.5}FeO_{3-\delta}$ were prepared via the glycine-nitrate process (GNP), a self-combustion method using glycine as fuel and nitrates of the metal components as oxidant.[20] In the course of GNP, glycine was added in an aqueous nitrate solution containing metal cations in the stoichiometric proportion; the glycine/nitrate molar ratio was 1.7–2.0 of stoichiometric, calculated assuming the only gaseous reaction products to be N_2, CO_2 and H_2O.

Table 1
Properties of ferrite-based ceramics

Composition	Additive (mol%)	Secondary phases	Crystal lattice[a]	Density (g/cm^3)	Perovskite unit cell parameters	
					a (nm)	α (°)
$La_{0.5}Sr_{0.5}FeO_{3-\delta}$	–	–	R	5.83	0.5493	60.27
$La_{0.5}Sr_{0.5}FeO_{3-\delta}$	Al_2O_3 (5.0%)	$SrAl_2O_4$	R	5.61	0.5503	59.98
$La_{0.5}Sr_{0.5}FeO_{3-\delta}$	$SrAl_2O_4$ (5.3%)	$SrAl_2O_4$	R	5.71	0.5491	60.25
$(La_{0.5}Sr_{0.5})_{0.97}FeO_{3-\delta}$	–	–	R	5.87	0.5497	60.12
$La_{0.5}Sr_{0.5}Fe_{0.9}Al_{0.1}O_{3-\delta}$	–	–	R	5.72	0.5491	59.99
$La_{0.3}Sr_{0.7}FeO_{3-\delta}$	–	–	C	5.49	0.3872	–
$La_{0.2}Sr_{0.8}Fe_{0.8}Ga_{0.2}O_{3-\delta}$	–	–	C	5.32	0.3888	–
$La_{0.2}Sr_{0.8}Fe_{0.8}Ga_{0.2}O_{3-\delta}$	Al_2O_3 (5.0%)	$SrAl_2O_4$, $SrLaGa_3O_7$	C	5.37	0.3881	–
$SrFe_{0.7}Al_{0.3}O_{3-\delta}$	–	–	C	4.42	0.3900	–
$SrFe_{0.7}Al_{0.3}O_{3-\delta}$	Al_2O_3 (5.0%)	$SrAl_2O_4$	C	4.49	0.3890	–

Composition	Additive	Average TECs in air		Activation energy for oxygen permeation[b]	
		T (K)	$\bar{\alpha} \times 10^6$ (K^{-1})	T (K)	E_A (kJ/mol)
$La_{0.5}Sr_{0.5}FeO_{3-\delta}$	–	350–950	12.4	1023–1223	138 ± 13
		950–1310	23.7		
$La_{0.5}Sr_{0.5}FeO_{3-\delta}$	Al_2O_3	350–900	12.7	1023–1223	131 ± 16
		900–1300	25.6		
		1300–1500	21.0		
$La_{0.5}Sr_{0.5}FeO_{3-\delta}$	$SrAl_2O_4$	340–950	12.9	1023–1223	142 ± 8
		950–1150	24.1		
$(La_{0.5}Sr_{0.5})_{0.97}FeO_{3-\delta}$	–	350–950	12.4	1123–1223	111 ± 27
		950–1150	16.4		
$La_{0.5}Sr_{0.5}Fe_{0.9}Al_{0.1}O_{3-\delta}$	–	350–900	13.0	1073–1223	112 ± 13
		900–1200	27.6		
		1200–1500	22.0		
$La_{0.3}Sr_{0.7}FeO_{3-\delta}$	–	300–770	13.0	1023–1223	161 ± 12
		770–1150	24.9		
$La_{0.2}Sr_{0.8}Fe_{0.8}Ga_{0.2}O_{3-\delta}$	–	370–800	16.0	1023–1223	142 ± 7
		800–1080	26.7		
$La_{0.2}Sr_{0.8}Fe_{0.8}Ga_{0.2}O_{3-\delta}$	Al_2O_3	370–850	14.9	1023–1223	124 ± 15
		850–1200	25.2		
$SrFe_{0.7}Al_{0.3}O_{3-\delta}$	–	370–920	15.4	1123–1223	116 ± 18
		920–1270	23.0		
$SrFe_{0.7}Al_{0.3}O_{3-\delta}$	Al_2O_3	370–920	12.9	1123–1223	107 ± 22
		920–1270	19.8		

[a] C and R correspond to the cupic and rhombohedrally-distorted perovskite structures, respectively.
[b] The data correspond to the membrane thickness of 1.00 mm, $p_2 = 21$ kPa and $p_1 = 2.1$ kPa.

The solutions were heated on a hot plate until self-combustion, which started in the course of gradual heating up to 520–570 K. The resultant powders having a foamed structure were annealed at 1173–1373 K for 2 h to remove residual organic substances; selected portions of the powders were mixed with 5 mol% Al_2O_3 (99.99%). The samples of $La_{0.2}Sr_{0.8}Fe_{0.8}Ga_{0.2}O_{3-\delta}$ were prepared by a standard solid-state synthesis procedure, dissolving stoichiometric amounts of metal nitrates and carbonates in nitric acid; after drying on a hot plate, the nitrate mixture was decomposed in the course of slow heating up to 970 K in air. The resultant powder was milled and the solid state reaction was conducted in air at 1470–1640 K for 15 h with several intermediate grinding steps. The formation of single phase with a perovskite-type structure was confirmed by X-ray diffraction (XRD) analysis. Then 5% alumina was added to the powder, as for $SrFe_{0.7}Al_{0.3}O_{3-\delta}$ and $La_{0.5}Sr_{0.5}FeO_{3-\delta}$.

For all other ferrite-based materials listed in Table 1 and used in this work for comparison, the synthesis procedure was similar to that of $La_{0.2}Sr_{0.8}Fe_{0.8}Ga_{0.2}O_{3-\delta}$. The only exception is $La_{0.5}Sr_{0.5}Fe_{0.9}Al_{0.1}O_{3-\delta}$, which was synthesized by GNP due to significant kinetic limitations hampering the formation of single perovskite-type phase in the course of solid state reactions. Finally, all powders were ball-milled in ethanol or acetone; the particle size estimated by the scanning electron microscopy (SEM), varied in the range 30–120 nm for the GNP-synthesized powders and 80–500 nm for the samples prepared by the standard ceramic route. Gas-tight ceramics were uniaxially pressed in the shape of disks (diameter of 1.0–1.8 cm; pressure of 120–400 MPa) and sintered at 1490–1770 K in air for 2–8 h. The dependency of the ceramic density on the sintering conditions is discussed below. Then the samples were polished, annealed in air at 1170–1270 K for 2–3 h and slowly furnace-cooled to achieve equilibrium with air at low temperatures. The tubular membranes were compacted by cold isostatic pressing (CIP) using a Burton Corblin instrument (France), with pressure vessel of 90 mm in diameter and 500 mm in length.

The materials were characterized by scanning electron microscopy combined with energy dispersive spectroscopy (SEM/EDS), inductively-coupled plasma (ICP) spectroscopic analysis, standard picnometric technique, dilatometry, and steady-state oxygen permeation and total conductivity (4-probe DC) measurements. The XRD patterns were collected at room temperature using a Rigaku D/MAX-B diffractometer (Cu Kα, $2\Theta = 20°$–$80°$, step 0.02°, 1 s/step). Thermal expansion and shrinkage were measured using an alumina Linseis L70 dilatometer with a constant heating rate of 5 °C/min, in air. SEM studies were performed using a Hitachi S-4100 microscope equipped with a Rontec UHV Detection system for the EDS analysis. Only gas-tight samples were used for the permeation studies. All data on oxygen permeability presented in this work correspond to the membrane feed-side oxygen partial pressure (p_2) maintained at 21 kPa (atmospheric air); the permeate-side oxygen partial pressure (p_1) varied in the range 0.2–20 kPa. Detailed description of the equipment and techniques, used for ceramic characterization and oxygen permeation measurements, was published earlier (see 7,9,10,21,22 and references cited).

3. Results and discussion

3.1. Sintering of ferrite-based ceramics with alumina additions: $La_{0.5}Sr_{0.5}FeO_{3-\delta}$ and $SrFe_{0.7}Al_{0.3}O_{3-\delta}$

Dilatometric studies showed that, indeed, 5 mol% Al_2O_3 addition to $La_{0.5}Sr_{0.5}FeO_{3-\delta}$ powder results in a considerably higher sinterability (Fig. 1) and a smaller grain size (Fig. 2). In contrast to the undoped ferrite, extensive sintering processes in the presence of alumina start at 1000–1200 K. The maximum density is achieved at approximately 1570 K (Fig. 3A). At the same time, the sintered material is almost single-phase (Fig. 4). In fact, very small impurity peaks characteristic of $SrAl_2O_4$ phase are only visible in the course of a high-resolution XRD scan. The unit cell volume of the perovskite phase formed in $La_{0.5}Sr_{0.5}FeO_{3-\delta}$–$Al_2O_3$ ceramics is larger with respect to undoped lanthanum-strontium ferrite, whilst the rhombohedral distortion characteristic of $La_{0.5}Sr_{0.5}FeO_{3-\delta}$ structure decreases to an almost negligible level (Table 1). These data suggest that a major part of alumina is dissolved in the ferrite lattice during sintering, leading to the formation of A-site deficient perovskite. The creation of A-site cation vacancies is accompanied with increasing coulombic repulsion of oxygen anions and, thus, with the expansion of the perovskite unit cell; a similar effect may also be expected for the A-site deficiency charge compensation mechanism via oxygen vacancy formation. Nonetheless, the traces of secondary alumina-rich phase are still present at the grain boundaries (Fig. 2B and C).

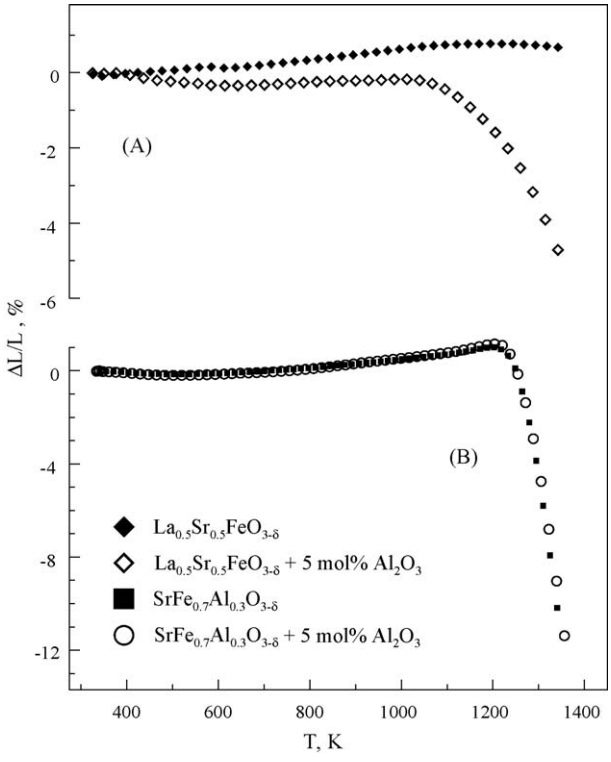

Fig. 1. Shrinkage curves for $La_{0.5}Sr_{0.5}FeO_3$- and $SrFe_{0.7}Al_{0.3}O_3$-based green compacts.

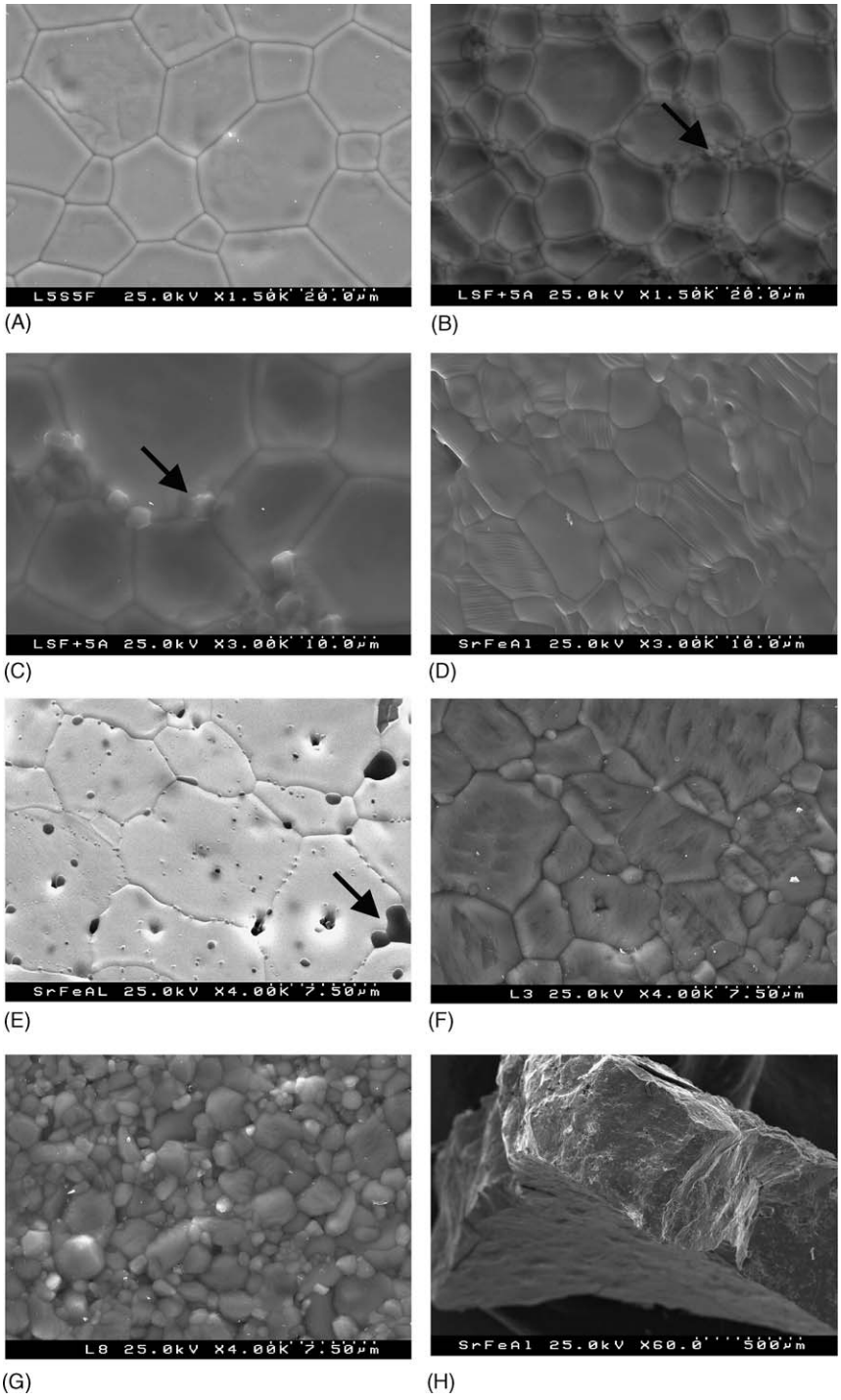

Fig. 2. SEM micrographs of $La_{0.5}Sr_{0.5}FeO_{3-\delta}$ (A), $La_{0.5}Sr_{0.5}FeO_{3-\delta}$ with Al_2O_3 (B and C), $SrFe_{0.7}Al_{0.3}O_{3-\delta}$ (D), $SrFe_{0.7}Al_{0.3}O_{3-\delta}$ with Al_2O_3 addition (E), $La_{0.2}Sr_{0.8}Fe_{0.8}Ga_{0.2}O_{3-\delta}$ (F), $La_{0.2}Sr_{0.8}Fe_{0.8}Ga_{0.2}O_{3-\delta}$ with Al_2O_3 addition (G), and fractured $SrFe_{0.7}Al_{0.3}O_{3-\delta}$–$Al_2O_3$ composite tube (H). The arrows show alumina-rich precipitates in $La_{0.5}Sr_{0.5}FeO_{3-\delta}$- and $SrFe_{0.7}Al_{0.3}O_{3-\delta}$-based materials, detected by EDS (B, C and E).

In the case of $SrFe_{0.7}Al_{0.3}O_{3-\delta}$, no essential influence of alumina additions on the shrinkage was found at temperatures below 1370 K (Fig. 1). At higher temperatures, however, another situation is observed. For single-phase $SrFe_{0.7}Al_{0.3}O_{3-\delta}$ ceramics, the highest density could be obtained at 1473–1523 K (Fig. 3A); further increase of the sintering temperature rises grain size and total porosity. Although the atomic weight of Al is low compared to Sr and Fe, adding 5 mol% (3 wt.%) alumina makes it possible to increase the density (Fig. 3B). For the materials with the addition sintered at 1623 K for 3–4 h, the density is even higher than that of single-phase $SrFe_{0.7}Al_{0.3}O_{3-\delta}$. The XRD and SEM/EDS analyses showed the presence of a secondary phase, $SrAl_2O_4$, the amount of which is substantially larger than that in Al_2O_3-containing $La_{0.5}Sr_{0.5}FeO_{3-\delta}$ (Figs. 2E and 4). Despite the formation of A-site cation vacancies in the cubic perovskite Sr(Fe, Al)$O_{3-\delta}$, alumina addition

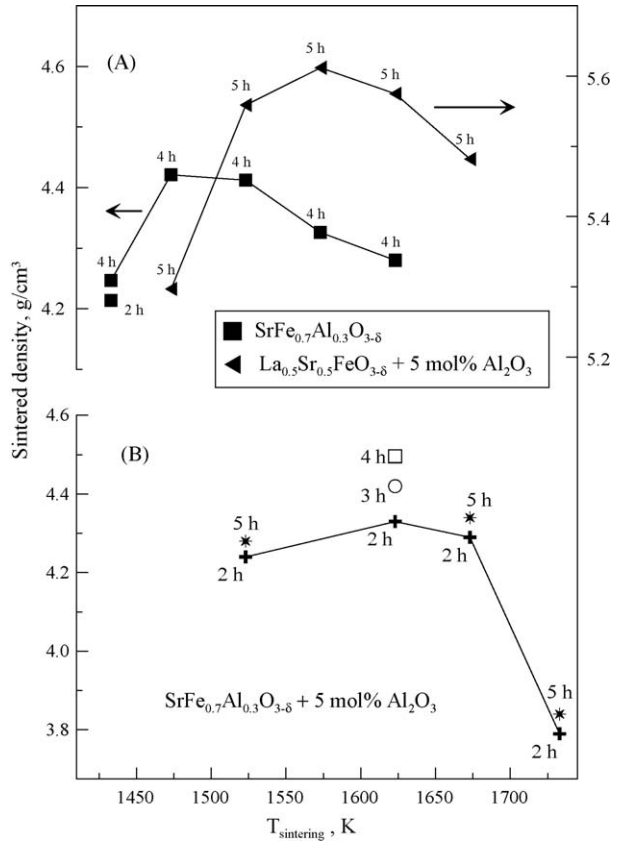

Fig. 3. Density of ferrite-based materials as a function of the sintering temperature and time: $SrFe_{0.7}Al_{0.3}O_{3-\delta}$ and $La_{0.5}Sr_{0.5}FeO_{3-\delta}$–$Al_2O_3$ (A), and $SrFe_{0.7}Al_{0.3}O_{3-\delta}$–$Al_2O_3$ (B).

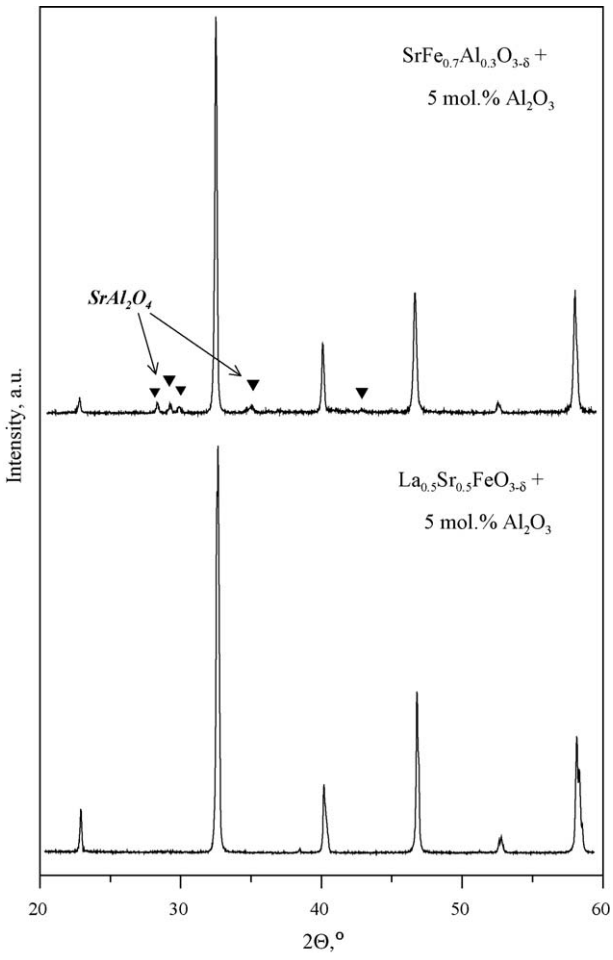

Fig. 4. XRD patterns of sintered $La_{0.5}Sr_{0.5}FeO_{3-\delta}$ and $SrFe_{0.7}Al_{0.3}O_{3-\delta}$ ceramics with Al_2O_3 addition.

leads to the unit cell contraction (Table 1) indicating a substantial change in the state of iron cations. More detailed studies of the charge compensation mechanism are necessary to identify exact reasons responsible for this behavior.

In general, the improved sinterability of both $La_{0.5}Sr_{0.5}FeO_{3-\delta}$–$Al_2O_3$ and $SrFe_{0.7}Al_{0.3}O_{3-\delta}$–$Al_2O_3$ ceramics seems closely associated with the interaction between perovskite phases and alumina. In the case of $La_{0.5}Sr_{0.5}FeO_{3-\delta}$, this solid-state interaction is more extensive and should involve, at least, Al^{3+} diffusion into the perovskite and strontium cations transfer towards alumina particles to form $SrAl_2O_4$. For $SrFe_{0.7}Al_{0.3}O_{3-\delta}$ where the aluminum content is close to the solubility limit,[9] the latter process is expected to prevail and the overall driving force for cation interdiffusion should be substantially lower than that in $La_{0.5}Sr_{0.5}FeO_{3-\delta}$–$Al_2O_3$ system. At the same time, one should note that the solid-state interaction might not be considered as the only process responsible for the sintering changes. Additional studies are necessary to identify other relevant factors, particularly the role of $SrAl_2O_4$ precipitates in the grain growth processes.

3.2. Conductivity and thermal expansion

The results on total conductivity (Fig. 5), which is predominantly p-type electronic,[8,9] support the above conclusion. Alumina addition to $SrFe_{0.7}Al_{0.3}O_{3-\delta}$ decreases slightly the conductivity of dual-phase ceramics, but this influence is rather negligible. Such behavior indicates that the hole concentration and mobility are essentially unaffected by the changes in the perovskite phase composition, whereas the amount of segregated $SrAl_2O_4$ is lower than the percolation threshold. In the case of Al_2O_3-doped $La_{0.5}Sr_{0.5}FeO_{3-\delta}$, the conductivity decreases 1.5–3.2 times with respect to pure ferrite due to the dominant dissolution of Al^{3+} cations in the lattice, decreasing the total concentration of B sites participating in the electronic transport. Taking into account the data on Ga- and Al-substituted ferrites with perovskite structure,[23,24] one may also expect a decrease in the absolute concentration of electron holes localized on iron cations.

As for the total conductivity, the effects of Al_2O_3 additions on thermal expansion of $La_{0.5}Sr_{0.5}FeO_{3-\delta}$ and $SrFe_{0.7}Al_{0.3}O_{3-\delta}$ ceramics are drastically different (Fig. 6). For the latter composition, the average thermal expansion coefficient (TEC) decreased from $15.4 \times 10^{-6}\,K^{-1}$ down to $12.9 \times 10^{-6}\,K^{-1}$ at temperatures below 920 K, and from $23.0 \times 10^{-6}\,K^{-1}$ down to $19.8 \times 10^{-6}\,K^{-1}$ at 920–1270 K (Table 1). In the case of alumina-enriched $La_{0.5}Sr_{0.5}FeO_{3-\delta}$ where most alumina is dissolved in the ferrite phase, a moderate increase in TECs is even observed. This trend is similar to other Fe-containing perovskites

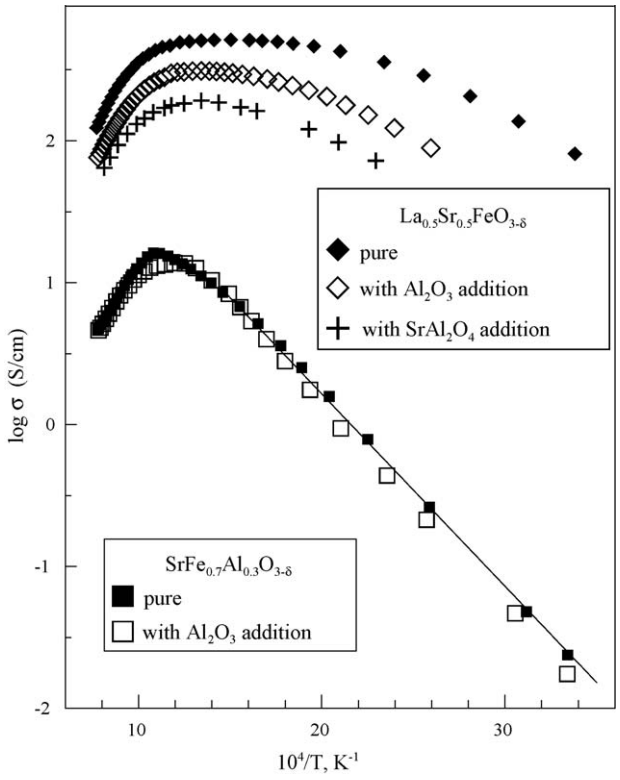

Fig. 5. Temperature dependence of the total conductivity of $La_{0.5}Sr_{0.5}FeO_3$- and $SrFe_{0.7}Al_{0.3}O_3$-based ceramics.

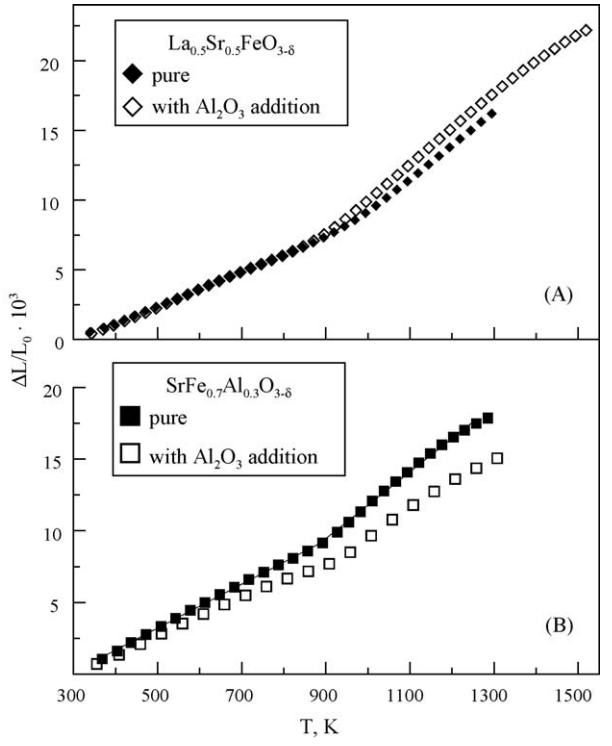

Fig. 6. Dilatometric curves of sintered $La_{0.5}Sr_{0.5}FeO_3$- and $SrFe_{0.7}Al_{0.3}O_3$-based ceramics in air.

with a significant A-site deficiency, such as $Sr_{1-x}(Fe,Ti)O_{3-\delta}$[25]; vacancies in a crystal lattice increase unharmonicity of atomic vibrations and may weaken metal-oxygen bonding,[21,26,27] in parallel with a possible change in the oxygen thermodynamic functions. Notice that for all these materials, the non-linearity of dilatometric curves at 750–950 K and the apparent increase in thermal expansion on heating are mainly due to the so-called chemical contribution, caused by extensive oxygen losses and the corresponding changes in the oxidation state and radius of iron cations when temperature increases.[21] It seems quite likely, therefore, that the creation of A-site vacancies and Al^{3+} incorporation into the iron sublattice of $La_{0.5}Sr_{0.5}FeO_{3-\delta}$ may influence oxygen thermodynamics, increasing the oxygen content variations at 900–1300 K.

3.3. Oxygen permeability

Fig. 7 shows the $p(O_2)$-dependencies of oxygen permeation fluxes, j, and specific oxygen permeabilities, $J(O_2)$, through dense ceramic membranes of Al_2O_3-doped $La_{0.5}Sr_{0.5}FeO_{3-\delta}$ with various thicknesses. The oxygen permeability values are calculated by[10,22]:

$$j = \frac{J(O_2)}{d}\left[\ln\frac{p_2}{p_1}\right] \quad (1)$$

where d is membrane thickness, and p_2 and p_1 are feed-side and permeate-side oxygen partial pressures, respectively. Since this term is proportional to $j \times d$, its value is thickness-independent when surface-exchange limitations are negligible but increases with thickness when they become significant[10,22].

The specific permeability of Al_2O_3-containing $La_{0.5}Sr_{0.5}FeO_{3-\delta}$ ceramics is almost thickness-independent at 1223 K (Fig. 7), indicating that oxygen transport at this temperature is limited mainly by bulk ionic conductivity. The role of surface limitations, however, increases with decreasing temperature and on reducing oxygen pressure. This suggests, in particular, that the activation energy (E_A) for ionic conduction is lower than that for the surface exchange rate. A similar behavior was also found for most other materials studied in the present work, including $La_{0.5}Sr_{0.5}FeO_{3-\delta}$ and $SrFe_{0.7}Al_{0.3}O_{3-\delta}$ (Fig. 8). One important consequence is that the oxygen permeation data at temperatures below 1200 K cannot be used for precise calculations of the bulk ionic conductivity and its activation energy. The effective E_A values for oxygen permeation (Table 1) comprise also the contribution of exchange rate activation energy, the role of which increases on decreasing temperature. Nevertheless, taking into account the well-known correlation between bulk oxygen diffusion and surface exchange,[28] one can expect that the relationships between membrane composition and oxygen permeability, observed in this work, reflect the variations of ionic conductivity of the perovskite phases, at least in the high-temperature range.

Oxygen permeation fluxes through selected ceramic materials at fixed $p(O_2)$ gradient are presented in Fig. 9 as a function of temperature. Alumina addition to $SrFe_{0.7}Al_{0.3}O_{3-\delta}$ increases permeation by approximately 10%. This effect is similar to

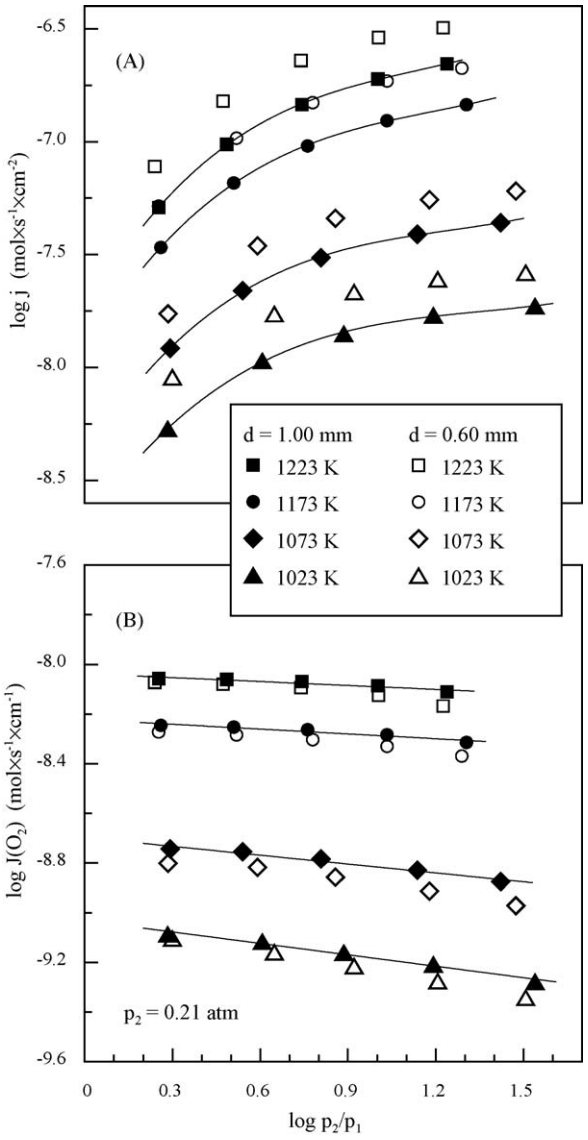

Fig. 7. Dependencies of the oxygen permeation fluxes (A) and specific permeability (B) of $La_{0.5}Sr_{0.5}FeO_{3-\delta}$–$Al_2O_3$ ceramics on the oxygen partial pressure gradient.

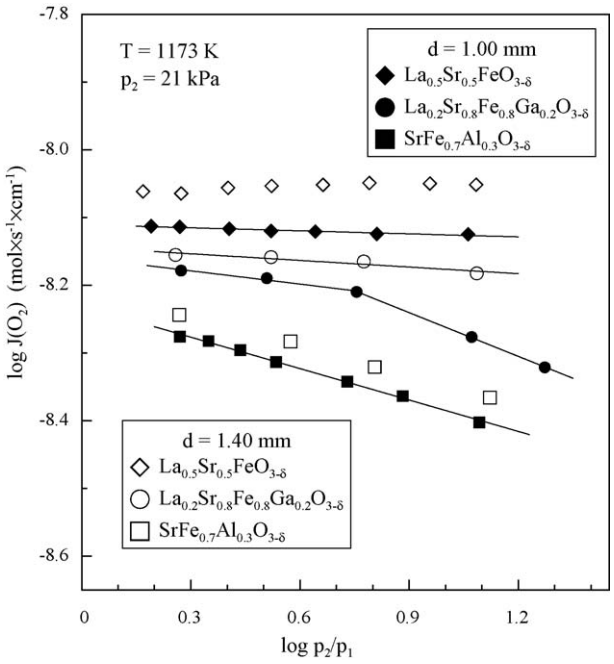

Fig. 8. Dependencies of the specific oxygen permeability of $La_{0.5}Sr_{0.5}FeO_{3-\delta}$, $SrFe_{0.7}Al_{0.3}O_{3-\delta}$ and $La_{0.2}Sr_{0.8}Fe_{0.8}Ga_{0.2}O_{3-\delta}$ ceramics on the oxygen partial pressure gradient at 1173 K.

that in strontium-deficient $Sr_{1-x}(Fe, Ti)O_{3-\delta}$ perovskites, where creation of the A-site vacancies promotes disorder in the oxygen sublattice and thus increases ionic conduction;[25] analogous tendencies were also reported for other perovskite-type compounds.[29]

In contrast, adding 5 mol% alumina to $La_{0.5}Sr_{0.5}FeO_{3-\delta}$ and the formation of Al-containing perovskite phase with A-site deficiency result in a substantially lower ionic transport. In order to assess compositional factors relevant for such decay, a series of single-phase perovskites including cation-deficient $(La_{0.5}Sr_{0.5})_{0.97}FeO_{3-\delta}$ and aluminum-substituted $La_{0.5}Sr_{0.5}Fe_{0.9}Al_{0.1}O_{3-\delta}$ were studied (Fig. 9). Both changes in the cation composition lead to decreasing oxygen permeability, suggesting a decrease in the ionic conductivity. Whilst the deteriorating influence of Al^{3+} incorporation on the ionic conduction in ferrites is well known,[9,10] the negative role of A-site vacancies in the case of $La_{0.5}Sr_{0.5}FeO_{3-\delta}$ may be asso-

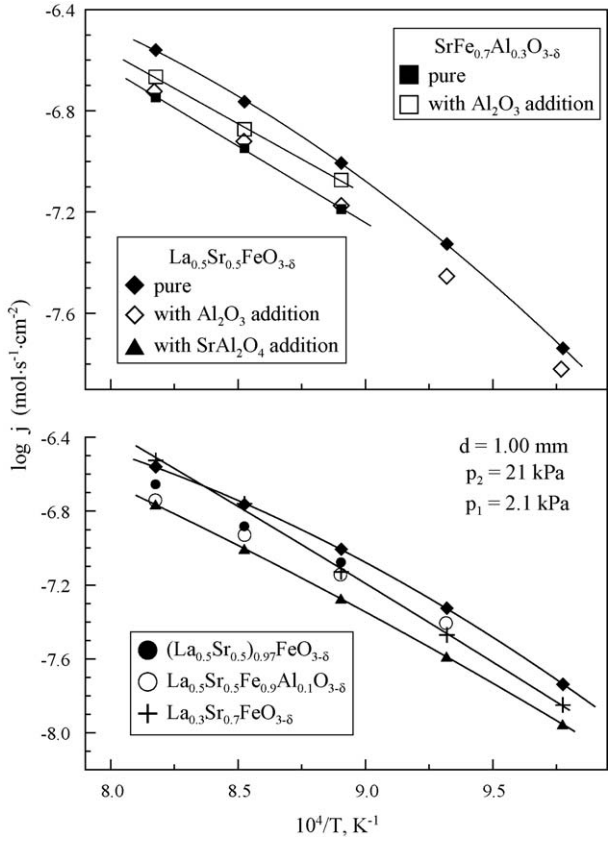

Fig. 9. Temperature dependencies of the oxygen permeation fluxes through ferrite-based membranes under fixed oxygen pressure gradient.

ciated with a relatively high disorder in the oxygen sublattice of this phase when compared to the $SrFeO_3$-based materials, such as $Sr(Fe,Al)O_{3-\delta}$ and $Sr(Fe, Ti)O_{3-\delta}$. For the latter group of mixed conductors, the phenomena related to formation of oxygen vacancy-ordered microdomains are even observed under oxidizing conditions at temperatures as high as 1100–1200 K (e.g. 9,22,25,30); the disordering processes induced by the A-site deficiency occur due to local distortion of the lattice near the cation vacancies, statistically distributed in the lattice. As the oxygen sublattice of $La_{0.5}Sr_{0.5}FeO_{3-\delta}$ is essentially disordered [8], the local structural distortions decrease ion mobility.

The oxygen permeability of $La_{0.5}Sr_{0.5}FeO_{3-\delta}$ ceramics sintered with addition of $SrAl_2O_4$, is also lower than that of undoped ferrite. In complement to the factors discussed above, partial dissolution of $SrAl_2O_4$ in the perovskite lattice should moderately shift the La:Sr concentration ratio towards lower values. Again, such a shift decreases ionic transport, as illustrated in Fig. 9 by the example of $La_{0.3}Sr_{0.7}FeO_{3-\delta}$.

3.4. Effect of Al_2O_3 addition on microstructure and oxygen permeability of $La_{0.2}Sr_{0.8}Fe_{0.8}Ga_{0.2}O_{3-\delta}$ ceramics

The results on $La_{0.5}Sr_{0.5}FeO_{3-\delta}$ and $SrFe_{0.7}Al_{0.3}O_{3-\delta}$ ceramics make it possible to conclude that, despite the enhancement in sinterability, the use of Al_2O_3 as a sintering aid may only be reasonable for the ferrite mixed conductors where the composition of perovskite-related phase prevents substantial dissolution of alumina. Also, a positive influence of this doping on the bulk ionic transport is only expected when the concentration of mobile oxygen vacancies may be increased due to the A-site cation deficiency resultant from the interaction between perovskite ferrites and Al_2O_3. For (La, Sr)FeO_3-based solid solutions, the latter situation takes place for highly oxygen-deficient materials derived from $SrFeO_{3-\delta}$, where most vacancies are trapped in ordered microdomains. Obviously, the above conclusions are related to SiO_2-uncontaminated ceramics, where the silica-scavenging effects of Al_2O_3 additions[15,16] have no key importance. On the other hand, microstructural modification of the ceramic surface, particularly increasing grain- and phase-boundary concentration at the surface due to Al_2O_3 additions, may be of interest for possible enhancement of the surface exchange kinetics.[31] For instance, the apparent activation energy for oxygen permeation through the alumina-doped membranes is systematically lower with respect to single-phase materials (Table 1); this may suggest a lower limiting effect of the exchange processes.

In order to verify these statements, pure and Al_2O_3-doped ceramics of $La_{0.2}Sr_{0.8}Fe_{0.8}Ga_{0.2}O_{3-\delta}$ were prepared and characterized. In this material, the content of Ga^{3+} is close to the solid solution formation limit[7] and further dissolution of Al^{3+} in the lattice should, hence, be insignificant. The XRD inspection revealed that alumina addition leads to segregation of two phases, $SrAl_2O_4$ and $SrLaGa_3O_7$; formation of the latter compound results probably from decreasing stability of $Sr(La)Fe(Ga)O_{3-\delta}$ solid solution, associated with the appearance of A-site cation deficiency. This is accompanied with noticeable microstructural changes,

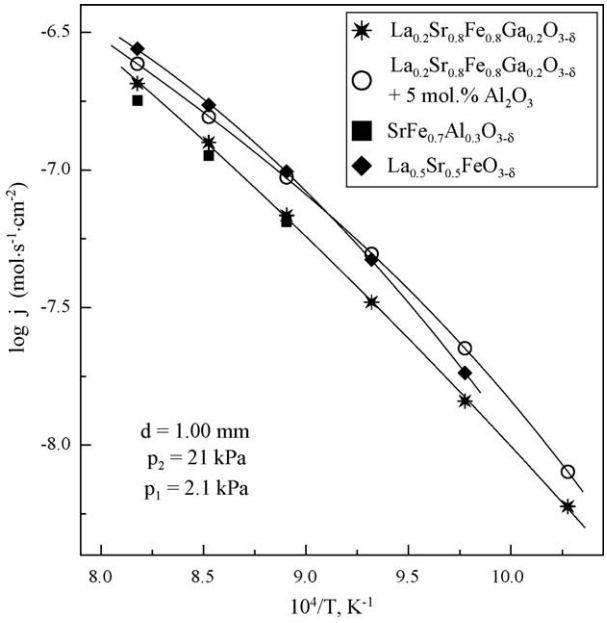

Fig. 10. Comparison of the oxygen permeation fluxes through $La_{0.2}Sr_{0.8}Fe_{0.8}Ga_{0.2}O_{3-\delta}$, $La_{0.2}Sr_{0.8}Fe_{0.8}Ga_{0.2}O_{3-\delta}$–$Al_2O_3$, $La_{0.5}Sr_{0.5}FeO_{3-\delta}$ and $SrFe_{0.7}Al_{0.3}O_{3-\delta}$ ceramics under fixed oxygen pressure gradient.

in particular decreasing grain size (Fig. 2F and G). The cubic perovskite unit cell volume, the average TECs, and the effective activation energy for oxygen permeation all decrease on doping, as for Al_2O_3-enriched $SrFe_{0.7}Al_{0.3}O_{3-\delta}$ (Table 1). The minor alumina addition substantially increases oxygen permeation fluxes; at 973-1073 K the permeability of Al_2O_3-doped $La_{0.2}Sr_{0.8}Fe_{0.8}Ga_{0.2}O_{3-\delta}$ is higher than that of single-phase $La_{0.5}Sr_{0.5}FeO_{3-\delta}$ (Fig. 10). Thus, the similar behavior observed for $SrFe_{0.7}Al_{0.3}O_{3-\delta}$–$Al_2O_3$ and $La_{0.2}Sr_{0.8}Fe_{0.8}Ga_{0.2}O_{3-\delta}$–$Al_2O_3$ ceramics supports the relevance of the mechanisms discussed above.

Although the $La_{0.2}Sr_{0.8}Fe_{0.8}Ga_{0.2}O_{3-\delta}$–$Al_2O_3$ material exhibits faster oxygen transport with respect to its $SrFe_{0.7}Al_{0.3}O_3$-based analogue, the latter composition is strongly preferable, however, in terms of the costs of raw materials. Also, the presence of Ga^{3+} cations in mixed-conducting ceramic membranes may decrease chemical stability in reducing atmospheres due to possible volatilization of gallium oxide and interaction with catalysts, such as Pt or Ni.[32] Therefore, for the fabrication of tubular membranes used in a model reactor for natural gas conversion, the composition comprising $SrFe_{0.7}Al_{0.3}O_{3-\delta}$ and 5 mol% (3 wt.%) Al_2O_3 was selected. Fig. 11 shows the high-quality ceramic tubes, compacted by CIP at 175 MPa and sintered at 1623 K for 3–4 h. In the course of processing, the ball-milled powder was filled around a steel mandrel (diameter of 6.35 mm) in a flexible latex rubber hose; special care was taken to distribute the powder symmetrically around the mandrel in order to avoid as much as possible eccentricity, i.e. variation of circular wall thickness. The gas-tight tubes have the inner diameter of 5 mm and wall thickness of 0.7–1.2 mm (Figs. 2E and 11). Long-term stability tests of $SrFe_{0.7}Al_{0.3}O_3$–Al_2O_3 membranes under air/CH_4 gradient are now in progress.

Fig. 11. Dense tubular membranes of $SrFe_{0.7}Al_{0.3}O_{3-\delta}$ with Al_2O_3 addition.

4. Conclusions

Minor additions of Al_2O_3 to mixed-conducting materials based on perovskite-related ferrites make it possible to improve the sinterability of ceramics and, often, to decrease grain size. The effects of alumina doping on the oxygen permeation and thermal expansion are, however, strongly dependent on the solubility of Al^{3+} in the lattice and on the relationships between A-site cation deficiency and ionic transport. For (Sr, La)FeO_3-based systems, these factors are determined by the La:Sr concentration ratio and by the presence of dopant cations in the B sublattice. In the case of mixed conductors derived from strontium ferrite, such as $SrFe_{0.7}Al_{0.3}O_{3-\delta}$ and $La_{0.2}Sr_{0.8}Fe_{0.8}Ga_{0.2}O_{3-\delta}$ where the composition is close to the solid solution formation limits and local oxygen-vacancy ordering plays important role, Al_2O_3 additions result in the segregation of $SrAl_2O_4$, increasing oxygen ionic conduction due to the creation of A-site vacancies statistically distributed in the structure, and in decreasing thermal expansion. In the case of $La_{0.5}Sr_{0.5}FeO_{3-\delta}$, the substitution of iron with aluminum cations, deficiency of the A sublattice, and changing the La:Sr concentration ratio all decrease ionic conductivity. As a result, additions of either Al_2O_3 or $SrAl_2O_4$ have a negative influence on the oxygen permeation fluxes through $La_{0.5}Sr_{0.5}FeO_3$-based membranes.

Acknowledgements

This work was supported by the FCT, Portugal (projects POCI/CTM/58570/2004 and BD/6595/2001), by the NATO Science for Peace program (project 978002), by the COST 525 "Advanced Electroceramics: Grain Boundary Engineering" program (CEC), and by the Belarus Ministry of Education and Science.

References

1. Dyer, P. N., Richards, R. E., Russek, S. L. and Taylor, D. M., Ion transport membrane technology for oxygen separation and syngas production. *Solid State Ionics*, 2000, **134**, 21.
2. Mazanec, T. J., Electropox gas reforming. In *LiuCeramic Membranes I*, ed. H. U. Anderson, A. C. Khandar and M. Liu. The Electrochemical Society, Pennington, NJ, 1997, PV95-24, p. 16.
3. Pei, S., Kleefisch, M. S., Kobylinski, T. P., Faber, J., Udovich, C. A., Zhang-McCoy, V. *et al.*, Failure mechanisms of ceramic membrane reactors in partial oxidation of methane to synthesis gas. *Catal. Lett.*, 1995, **30**, 201.
4. Schwartz, M., White, J. H. and Sammells, A. F., *Solid state oxygen anion and electron mediating membrane and catalytic membrane reactors containing them*, US Patent 6214757, 2001.
5. Hendriksen, P. V., Larsen, P. H., Mogensen, M., Poulsen, F. W. and Wiik, K., Prospects and problems of dense oxygen permeable membranes. *Catal. Today*, 2000, **56**, 283.
6. George, C., Majkic, G., Lo, W. and Salama, K., Processing of dense $La_{0.2}La_{0.8}Fe_{0.8}Cr_{0.2}O_{3-\delta}$ oxygen membranes. *Mater. Sci. Eng. B*, 2001, **83**, 198.
7. Kharton, V. V., Shaula, A. L., Viskup, A. P., Avdeev, M. Yu., Yaremchenko, A. A., Patrakeev, M. V. *et al.*, Perovskite-like system (Sr, La)(Fe, Ga)$O_{3-\delta}$: structure and ionic transport under oxidizing conditions. *Solid State Ionics*, 2002, **150**, 229.
8. Patrakeev, M. V., Bahteeva, J. A., Mitberg, E. B., Leonidov, I. A., Kozhevnikov, V. L. and Poeppelmeier, K. R., Electron/hole and ion transport in $La_{1-x}Sr_xFeO_{3-\delta}$. *J. Solid State Chem.*, 2003, **172**, 219.
9. Shaula, A. L., Kharton, V. V., Patrakeev, M. V., Waerenborgh, J. C., Rojas, D. P. and Marques, F. M. B., Defect formation and transport in $SrFe_{1-x}Al_xO_{3-\delta}$. *Ionics*, 2004, **10**, 378.
10. Kharton, V. V., Yaremchenko, A. A., Shaula, A. L., Viskup, A. P., Marques, F. M. B., Frade, J. R. *et al.*, Oxygen permeability and thermal expansion of ferrite-based mixed conducting ceramics. *Defect Diffus. Forum*, 2004, **226–228**, 141.
11. Mims, C. A., Bayani, N., Jacobson, A. J. and van der Heide, P. A. W., Modes of oxygen exchange in $La_{0.2}La_{0.8}Fe_{0.8}Cr_{0.2}O_{3-\delta}$. *Solid State Ionics*, 2005, **176**, 319.
12. Kharton, V. V., Yaremchenko, A. A., Valente, A. A., Sobyanin, V. A., Belyaev, V. D., Semin, G. L. *et al.*, Methane oxidation over Fe-, Co-, Ni- and V-containing mixed conductors. *Solid State Ionics*, 2005, **176**, 781.
13. Lu, X. and Liu, M., Ferrite-based MIEC membranes for oxygen separation and methane conversion. In *Solid State Ionic Devices*, ed. E. Wachsman, J. R. Akridge, M. Liu and N. Yamazoe. The Electrochemical Society, Pennington, NJ, 1999, PV99-13, p. 139.
14. Frade, J. R., Kharton, V. V., Yaremchenko, A. A. and Naumovich, E. N., Methane to syngas conversion. Part I. Equilibrium conditions and stability requirements of membrane materials. *J. Power Sources*, 2004, **130**, 77.
15. Drennan, J. and Auchterlonie, G., Microstuctural aspects of oxygen ion conduction in solids. *Solid State Ionics*, 2000, **134**, 75.
16. Lee, J.-H., Mori, T., Li, J.-G., Ikegami, T., Komatsu, M. and Haneda, H., Improvement of grain-boundary conductivity of 8 mol% yttria-stabilized zirconia by precursor scavenging of siliceous phase. *J. Electrochem. Soc.*, 2000, **147**, 2822.
17. Yasuda, I., Matsuzaki, Y., Yamakawa, T. and Koyama, T., Electrical conductivity and mechanical properties of alumina-dispersed doped lanthanum gallates. *Solid State Ionics*, 2000, **135**, 381.
18. Jurado, J. R., Present several items on ceria-based ceramic electrolytes: synthesis, additive effects, reactivity and electrochemical behaviour. *J. Mater. Sci.*, 2001, **36**, 1133.
19. Steil, C. M., Fouletier, J., Kleitz, M., Lagrange, G., del Gallo, P., Mairesse, G. *et. al.*, *Process for preparing a composite electrolyte based on BIMEVOX and the use of said compound in separating oxygen from a gas mixture*. US Patent 6207038, 2001.
20. Chick, L. A., Pederson, L. R., Maupin, G. D., Bates, J. L., Thomas, L. E. and Exarhos, G. J., Glycine-nitrate combustion synthesis of oxide ceramic powders. *Mater. Lett.*, 1990, **10**, 6.
21. Kharton, V. V., Yaremchenko, A. A., Patrakeev, M. V., Naumovich, E. N. and Marques, F. M. B., Thermal and chemical induced expansion of $La_{0.3}Sr_{0.7}$(Fe, Ga)$O_{3-\delta}$ ceramics. *J. Eur. Ceram. Soc.*, 2003, **23**, 1417.
22. Kharton, V. V., Viskup, A. P., Kovalevsky, A. V., Figueiredo, F. M., Jurado, J. R., Yaremchenko, A. A. *et al.*, Surface-limited ionic transport in perovskites $Sr_{0.97}$(Ti, Fe, Mg)$O_{3-\delta}$. *J. Mater. Chem.*, 2000, **10**, 1161.

23. Waerenborgh, J. C., Rojas, D. P., Shaula, A. L., Mather, G. C., Patrakeev, M. V., Kharton, V. V. *et al.*, Phase formation and iron oxidation states in $SrFe(Al)O_{3-\delta}$ perovskites. *Mater. Lett.*, 2005, **59**, 1644.
24. Patrakeev, M. V., Mitberg, E. B., Lakhtin, A. A., Leonidov, I. A., Kozhevnikov, V. L., Kharton, V. V. *et al.*, Oxygen nonstoichiometry, conductivity and Seebeck coefficient of $La_{0.3}Sr_{0.7}Fe_{1-x}Ga_xO_{2.65+\delta}$ perovskites. *J. Solid State Chem.*, 2002, **167**, 203.
25. Kharton, V. V., Kovalevsky, A. V., Tsipis, E. V., Viskup, A. P., Naumovich, E. N., Jurado, J. R. *et al.*, Mixed conductivity and stability of A-site-deficient $Sr(Fe, Ti)O_{3-\delta}$ perovskites. *J. Solid State Electrochem.*, 2002, **7**, 30.
26. West, A. R., *Solid State Chemistry and its Applications*. John Wiley & Sons, Chichester, NY, Brisbane, 1984.
27. Hayashi, H., Kanoh, M., Quan, C. J., Inaba, H., Wang, S., Dokiya, M. *et al.*, Thermal expansion of Gd-doped ceria and reduced ceria. *Solid State Ionics*, 2000, **132**, 227.
28. Steele, B. C. H., Interfacial reactions associated with ceramic ion transport membranes. *Solid State Ionics*, 1995, **75**, 157.
29. Hatchwell, C., Bonanos, N. and Mogensen, M., The role of dopant concentration, A-site deficiency and processing on the electrical properties of strontium and titanium-doped lanthanum scandate. *Solid State Ionics*, 2004, **167**, 349.
30. Kharton, V. V., Waerenborgh, J. C., Rojas, D. P., Yaremchenko, A. A., Valente, A. A., Shaula, A. L. *et al.*, Mössbauer spectra and catalytic behavior of perovskite-like $SrFe_{0.7}Al_{0.3}O_{3-\delta}$. *Catal. Lett.*, 2005, **99**, 249.
31. Kharton, V. V., Yaremchenko, A. A., Tsipis, E. V., Valente, A. A., Patrakeev, M. V., Shaula, A. L. *et al.*, Characterization of mixed-conducting $La_2Ni_{0.9}Co_{0.1}O_{4+\delta}$ membranes for dry methane oxidation. *Appl. Catal. A*, 2004, **261**, 25.
32. Yamaji, K., Horita, T., Ishikawa, M., Sakai, N. and Yokokawa, H., Chemical stability of the $La_{0.9}Sr_{0.1}Ga_{0.8}Mg_{0.2}O_{2.85}$ electrolyte in a reducing atmosphere. *Solid State Ionics*, 1999, **121**, 217.